Article

Free Energy Barrier for Molecular Motions in Bistable [2]Rotaxane Molecular Electronic Devices

Hyungjun Kim, William A. Goddard III, Seung Soon Jang, William R. Dichtel, James R. Heath, and J. Fraser Stoddart

J. Phys. Chem. A, **2009**, 113 (10), 2136-2143• DOI: 10.1021/jp809213m • Publication Date (Web): 18 February 2009

Report Documentation Page

Form Approved
OMB No. 0704-0188

1. REPORT DATE	2. REPORT TYPE	3. DATES COVERED
12 JAN 2009		**00-00-2009 to 00-00-2009**

4. TITLE AND SUBTITLE	5a. CONTRACT NUMBER
Free Energy Barrier for Molecular Motions in Bistable [2]Rotaxane Molecular Electronic Devices	5b. GRANT NUMBER
	5c. PROGRAM ELEMENT NUMBER
6. AUTHOR(S)	5d. PROJECT NUMBER
	5e. TASK NUMBER
	5f. WORK UNIT NUMBER
7. PERFORMING ORGANIZATION NAME(S) AND ADDRESS(ES) **California Institute of Technology,Materials and Process Simulation Center,Pasadena,CA,91125**	8. PERFORMING ORGANIZATION REPORT NUMBER
9. SPONSORING/MONITORING AGENCY NAME(S) AND ADDRESS(ES)	10. SPONSOR/MONITOR'S ACRONYM(S)
	11. SPONSOR/MONITOR'S REPORT NUMBER(S)

12. DISTRIBUTION/AVAILABILITY STATEMENT
Approved for public release; distribution unlimited

13. SUPPLEMENTARY NOTES

14. ABSTRACT

15. SUBJECT TERMS

16. SECURITY CLASSIFICATION OF:			17. LIMITATION OF ABSTRACT	18. NUMBER OF PAGES	19a. NAME OF RESPONSIBLE PERSON
a. REPORT **unclassified**	b. ABSTRACT **unclassified**	c. THIS PAGE **unclassified**	**Same as Report (SAR)**	**9**	

Free Energy Barrier for Molecular Motions in Bistable [2]Rotaxane Molecular Electronic Devices†

Hyungjun Kim,‡ William A. Goddard III,*,‡ Seung Soon Jang,*,§ William R. Dichtel,||,⊥ James R. Heath,|| and J. Fraser Stoddart#

Materials and Process Simulation Center (MC 139-74), California Institute of Technology, Pasadena, California 91125, School of Materials Science and Engineering, Georgia Institute of Technology, Atlanta, Georgia 30332-0245, Division of Chemistry and Chemical Engineering (MC 127-72), California Institute of Technology, Pasadena, California 91125, Department of Chemistry and Biochemistry, University of California, Los Angeles, California, 90095-1569, and Department of Chemistry, Northwestern University, Evanston, Illinois 60208

Received: October 17, 2008; Revised Manuscript Received: January 12, 2009

Donor−acceptor binding of the π-electron-poor cyclophane cyclobis(paraquat-*p*-phenylene) ($CBPQT^{4+}$) with the π-electron-rich tetrathiafulvalene (TTF) and 1,5-dioxynaphthalene (DNP) stations provides the basis for electrochemically switchable, bistable [2]rotaxanes, which have been incorporated and operated within solid-state devices to form ultradense memory circuits (*ChemPhysChem* 2002, *3*, 519−525; *Nature* 2007, *445*, 414−417) and nanoelectromechanical systems. The rate of $CBPQT^{4+}$ shuttling at each oxidation state of the [2]rotaxane dictates critical write-and-retention time parameters within the devices, which can be tuned through chemical synthesis. To validate how well computational chemistry methods can estimate these rates for use in designing new devices, we used molecular dynamics simulations to calculate the free energy barrier for the shuttling of the $CBPQT^{4+}$ ring between the TTF and the DNP. The approach used here was to calculate the potential of mean force along the switching pathway, from which we calculated free energy barriers. These calculations find a turn-on time after the rotaxane is doubly oxidized of $\sim 10^{-7}$ s (suggesting that the much longer experimental turn-on time is determined by the time scale of oxidization). The return barrier from the DNP to the TTF leads to a predicted lifetime of 2.1 s, which is compatible with experiments.

1. Introduction

The electrochemically switchable, bistable [2]rotaxanes[1] (Figure 1) developed in recent years by Stoddart and co-workers exhibit two distinct co-conformations:[3−7] the ground-state co-conformation, in which the cyclobis(paraquat-*p*-phenylene) ($CBPQT^{4+}$) encircles the tetrathiafulvalene (TTF) station, and the metastable state co-conformation, in which the $CBPQT^{4+}$ encircles the 1,5-dioxynaphthalene (DNP) station.[2,8−15] The population of the two co-conformations may be shifted away from equilibrium by temporarily oxidizing one or two electrons from the TTF units. This switching process forms the basis of using these compounds as storage elements in molecular electronic devices. Consequently, significant experimental efforts have been made to investigate the switching behavior of molecular switches[5,6,16−23] and molecular machines[24−29] in various environments, such as solution,[5,6,30−37] polymer electrolyte gels,[38] metal surfaces[39−41] and devices.[7,16,17] Important experimental evidence[15] for molecular switching in these devices was the correlation of the kinetics of relaxation from the DNP to the TTF, across each of these environments. However, the rate of this process is also a function of the molecular structure, suggesting that longer storage times, or even nonvolatile memory, might be possible with the appropriate molecular design.

Computation chemistry calculations could provide an effective approach for optimizing the performance of such molecular switches, but such applications require that the accuracy of the theory be validated by comparing to well-documented experimental results. The purpose of this paper is to provide such validation. Previously, we investigated these compounds using a multiscale first principles approach combining quantum mechanics (QM) and atomistic force field (FF) methods.[42−47] First we considered the molecules as individual species, and then we examined self-assembled monolayers bound to gold surfaces or compressed into Langmuir monolayers at the air−water interface. These studies successfully predicted a number of phenomena that were confirmed later experimentally, including the higher conductivity[47] of the DNP relative to the TTF, and the increased stability of the TTF relative to the DNP (by 2.0 kcal/mol from QM, 2.3 kcal/mol from the FF, and 1.4−1.6 kcal/mol from experiment).[15,43] In addition, on the basis of the predicted footprint of the 115 $Å^2$/molecule for the self-assembled structure, we predicted that the surface tension of the TTF is 32% lower than that of the DNP, an observation that was confirmed in subsequent experiements.[43,44]

In this study, we evaluated the free energy profile of the shuttling motion of the $CBPQT^{4+}$ ring between the TTF and the DNP stations to determine how the nature of the rotaxane affects the switching and relaxation rates. These rates have been determined experimentally in various environments,[15,35,40,48] and

† Part of the "Max Wolfsberg Festschrift".

* To whom correspondence should be addressed. E-mail: W.A.G., wag@wag.caltech.edu; S.S.J., SeungSoon.Jang@mse.gatech.edu.

‡ Materials and Process Simulation Center (MC 139-74), California Institute of Technology.

§ Georgia Institute of Technology.

|| Division of Chemistry and Chemical Engineering (MC 127-72), California Institute of Technology.

⊥ University of California.

Northwestern University.

10.1021/jp809213m CCC: $40.75
Published on Web 02/18/2009

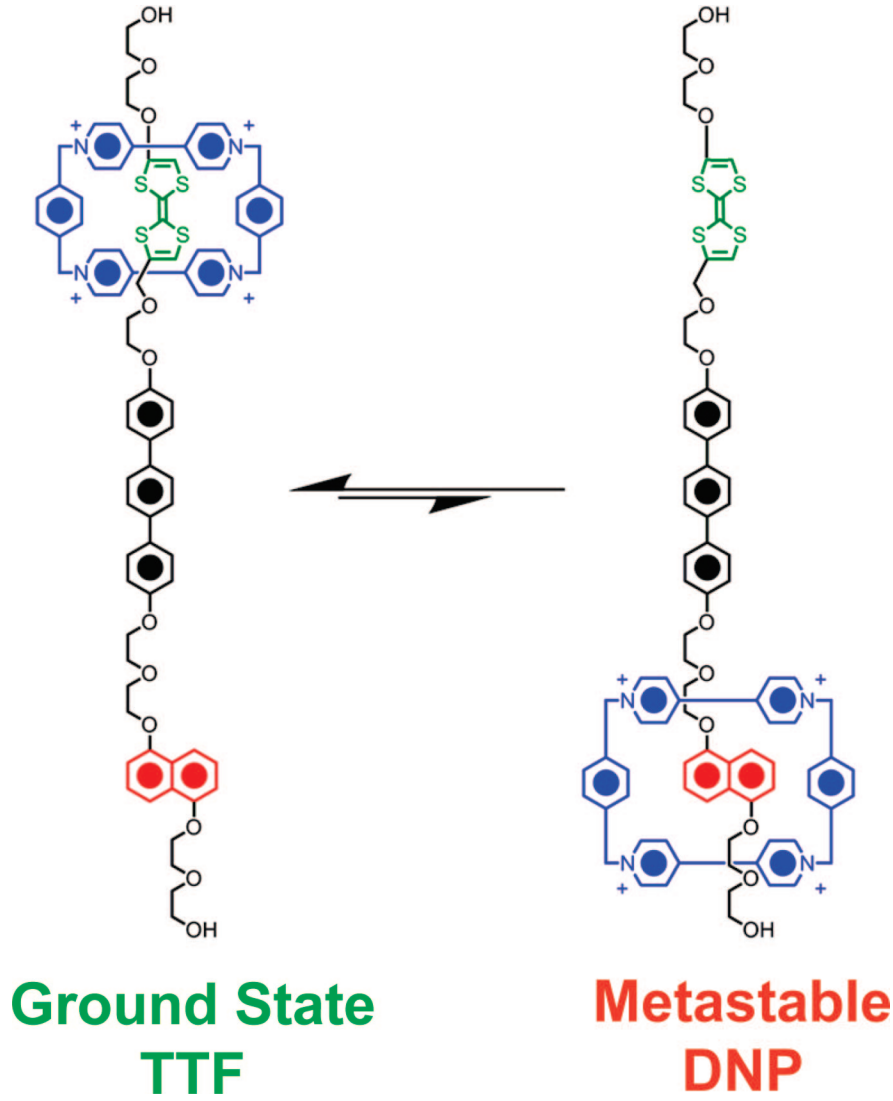

Figure 1. Structural formula of the two co-conformations of a bistable [2]rotaxane fragment used in this study.

we now want to understand the structural contributions to these rates. We seek to find a level for theoretical calculations of these rates that is both accurate and fast so that we can use theory to optimize the structural characteristics to achieve desired rates.

Rather than finding the energy barrier for a minimized reaction path connecting the two states, we used potential of mean force (PMF) to evaluate the change of free energy along the shuttling pathway of the $CBPQT^{4+}$ ring between the TTF and the DNP so that we can determine the rates at the experimental temperature. We carried out these calculations for three oxidation states of the molecule relevant to the switching and thermally activated relaxation process.

2. Simulation Details

2.1. Potential of Mean Force from Constrained Molecular Dynamics Simulation. The experimental time scale for the ring to relax back from the DNP to the TTF is 10^{-1}-10^{3} seconds,[15,34,49] suggesting that simple molecular dynamics (MD) simulation of a few hundred nanoseconds might not be sufficiently ergodic to provide an accurate transition rate. Hence, we adopted the "Blue Moon sampling" technique[50,51] of constrained MD simulations using holonomic constraints that fix the systems along the reaction coordinate. To determine the free energy barrier, we used the reaction-coordinate (R)-dependent potential of mean force (PMF), $F_{rxn}(R)$ defined as the integration of the mean force (MF) along the reaction coordinate, $-dF_{rxn}(R)/dR$.[52]

$$F_{rxn}(R) = F_{rxn}(\infty) + \int_{\infty}^{R} \frac{dF_{rxn}(R')}{dR'} dR' \qquad (1)$$

Here, the MF is a measurable quantity from our simulations. To calculate the MF, we assumed that the $CBPQT^{4+}$ ring moves between the TTF and the DNP along the backbone of the rotaxane (Figure 2a), which we assume to be in an extended conformation but with the minimized structure. This extended conformation should provide the fastest shuttling motion of the $CBPQT^{4+}$ ring, being governed mainly by its interaction with the backbone. This MF does not account for the presence of folded chain conformations, so that the PMF may lack some contributions from conformational entropy.

First, we prepared the extended rotaxane backbone *without* the $CBPQT^{4+}$ ring using quantum mechanical geometry optimization at the level of B3LYP/6-31G* (Figure 2a). Then, we added and optimized the $CBPQT^{4+}$ ring at various *fixed points* on the *fixed extended backbone* (Figure 2b) using quantum mechanics. Thus, the atomic partial charges of all atoms are allowed to readjust, depending on the relative position of the charge acceptor ($CBPQT^{4+}$) with respect to the charge donor (TTF and DNP).

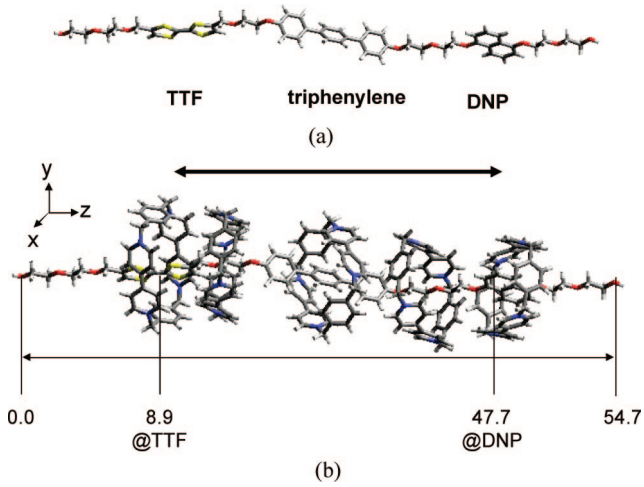

Figure 2. (a) Backbone of the rotaxane molecule simulated in this study. (b) $CBPQT^{4+}$ ring positions along the backbone (unit: Å).

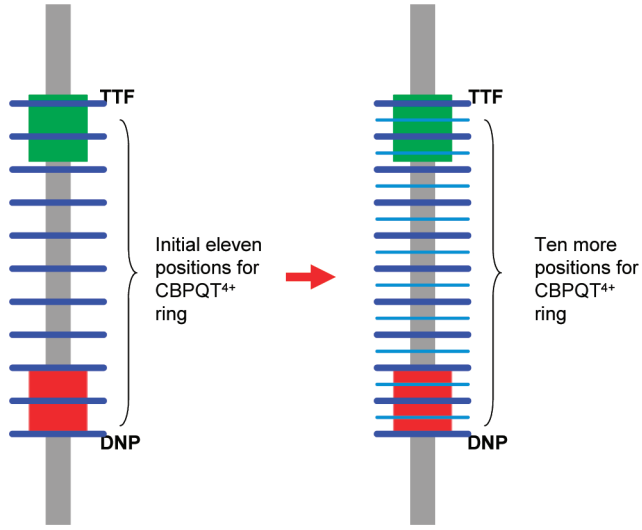

Figure 3. Charges for the initial nine structures obtained from QM with Mulliken analysis. In addition, we included two more structures beyond each station of the TTF and the DNP, using charges identical to those for the equilibrium $CBPQT^{4+}$@TTF and $CBPQT^{4+}$@DNP cases, respectively. Ten more structures were generated on the basis of these eleven structures. The position of the $CBPQT^{4+}$ ring for each additional structure was obtained using the arithmetic average of the two adjacent cases from the eleven structures. The charges were also averaged.

To obtain the change of the PMF during the shuttling process, we first evaluated the MF as a function of the position of the $CBPQT^{4+}$ ring. Because the length of the backbone is 54.7 Å and the distance between the TTF and the DNP is 36.9 Å, we chose to sample the dynamics for nine independent samples, each of which has the *z*-coordinate (along the backbone) of the center of mass (COM) of the $CBPQT^{4+}$ ring at a different position along the extended backbone, as schematically presented in Figure 3. Using quantum mechanics, the geometry and atomic charges were obtained from each of these nine cases.

After preparing these nine initial structures, we prepared two more structures beyond each station of the TTF and the DNP with identical charges to the $CBPQT^{4+}$@TTF case and the $CBPQT^{4+}$@DNP case, respectively. In addition, we constructed another ten structures in which the position and charges of the $CBPQT^{4+}$ ring were calculated by arithmetically averaging the coordinates and charges of two consecutive structures in the eleven structures. Thus, a total of 21 structures were prepared for simulations.

Then, to simulate both the turning on and turning off the rotaxane switch, we investigated the effect of oxidation of rotaxane molecule on the free energy profile, for three different oxidation states: the neutral state, the +1 oxidation state, and the +2 oxidation state.

The QM calculations of the charges for the nine different structures were repeated for each of the three oxidation states: 0, +1, and +2. The atomic partial charge distributions are tabulated in the Supporting Information, Table S1−S3.

All quantum mechanical computations in this study were performed using Jaguar.[53]

2.2. Constrained Molecular Dynamics Simulation. Next, we carried out a constrained NVT MD simulation at 300 K for 500 ps to equilibrate each system. This MD was then continued for an additional 3 ns at 300 K (constrained NVT MD) to compute the MF. The constraint was introduced using Gauss' principle of least constraints[54] to fix only the z-component of the center of mass (COM) of the $CBPQT^{4+}$ ring parallel to the molecular axis direction (z-axis direction as in Figure 2b). To ensure that our constraint dynamics produces the correct equilibrium averages without bias due to ensemble sampling, we used Fixman's theorem[55] to evaluate the metric effect originating from the holonomic constraints. We determined that the metric effect only adds a constant scalar value to the absolute free energy values, which has no influence on the relative energetics. (Details are in the Supporting Information.)

We also fixed the position of the last oxygen atom at each end of the backbone to retain the extended conformation. This restricts the conformational flexibility of the system, which suppresses conformational entropic contributions to the free energy. The mean force was sampled from such constrained MD simulations.

2.3. Force Field and MD Parameters. We used the generic DREIDING force field,[56] which was found to lead to accurate results in our previous studies on rotaxane systems.[43−45] It was also successful in our studies on various other molecular systems, such as the hydrated polymer electrolyte membranes[57−59] and the surfactant-mediated air−water interface.[60,61]

The force field has the form

$$E_{\text{total}} = E_{\text{vdW}} + E_{\text{Q}} + E_{\text{bond}} + E_{\text{angle}} + E_{\text{torsion}} + E_{\text{inversion}} \quad (2)$$

where E_{total}, E_{vdW}, E_{Q}, E_{bond}, E_{angle}, E_{torsion}, and $E_{\text{inversion}}$ are the total energies, the van der Waals, electrostatic, bond stretching, angle bending, torsion, and inversion energy components, respectively, and the force field parameters are described in the original papers.[56] The atomic charges were obtained from a QM Mulliken population analysis as indicated above.

All MD simulations were performed using LAMMPS (large-scale atomic/molecular massively parallel simulator) MD code from Plimpton at Sandia.[62,63] The equations of motion were integrated using the velocity−Verlet algorithm,[64] with a time step of 0.01 fs. This unusually small time step was to ensure high quality sampling of phase space by avoiding abrupt changes in atomic positions.

The temperature was kept constant during the MD using the Berendsen thermostat with temperature damping time of 0.01 fs. To demonstrate that our MD leads to a proper canonical ensemble, the probability distribution function (PDF) of kinetic energy KE ($=mv^2/2$) is shown in Figure 4. The PDF is quite close to the Maxwell−Boltzmann distribution of energy at $T =$ 300 K, indicating that the simulation describes a proper canonical ensemble. Furthermore, the PDF for each component

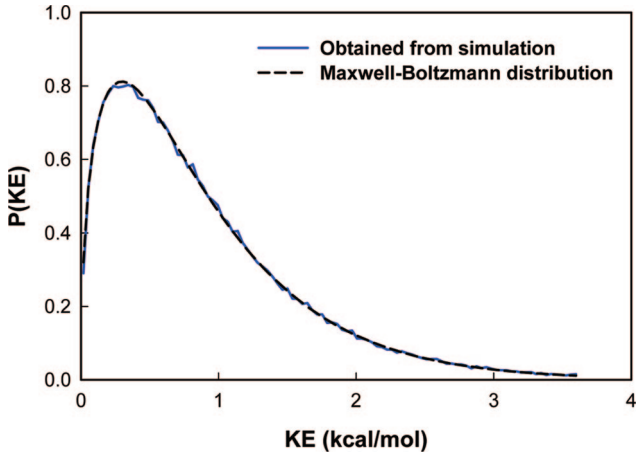

Figure 4. Probability density function of kinetic energy KE ($=mv^2/2$) is from the MD simulation of the CBPQT^{4+} ring@TTF (blue line) at 300 K. Here the time step was 0.01 fs and the total simulation time was 3 ns after 500 ps of equilibration. The black dashed line compares with the Maxwell−Boltzmann distribution of the energy, $2(\mathrm{KE}/\pi(k_BT)^3)^{1/2}\exp(-\mathrm{KE}/k_BT)$, for $T = 300$ K.

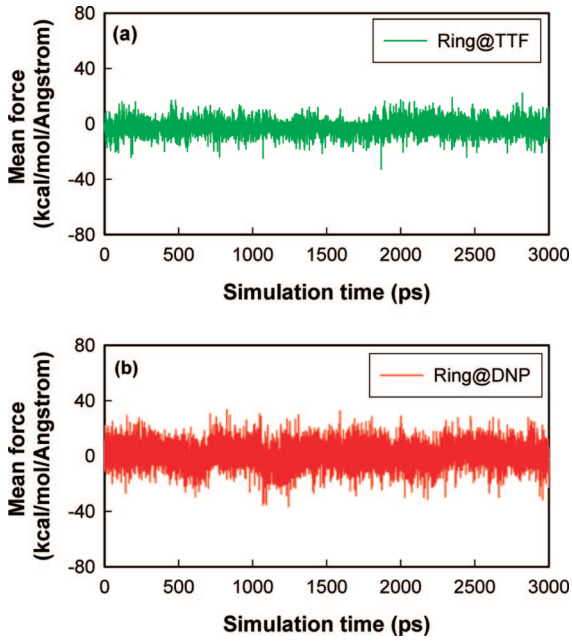

Figure 5. Change of mean force as a function of simulation time. In each case this follows 500 ps of equilibration time. This plot shows two representative cases: the CBPQT^{4+} ring@TTF (TTF) and the CBPQT^{4+} ring@DNP (DNP).

of velocity is the same and the system obeys the equipartition theorem (see Figure S1 in the Supporting Information).

Figure 5 shows the typical behavior of the MF as a function of simulation time for two representative systems: one is the ground state, CBPQT^{4+}@TTF, green color, denoted as TTF and the other is the metastable state, the CBPQT^{4+} ring on the DNP, red color, denoted as DNP. This shows that the mean force was well equilibrated for both cases.

The weakness of this blue moon sampling method is that the error in each MF measurement is integrated to obtain the PMF profile along the reaction coordinate. From block averages, we estimate the uncertainty of the MF values to be 0.04 (kcal/mol)/Å for CBPQT^{4+}@TTF and 0.22 (kcal/mol)/Å for CBPQT^{4+}@DNP. Assuming that these errors are random and that the average value is 0.13 (kcal/mol)/Å, we estimate that the error of the free energy difference between two stations is

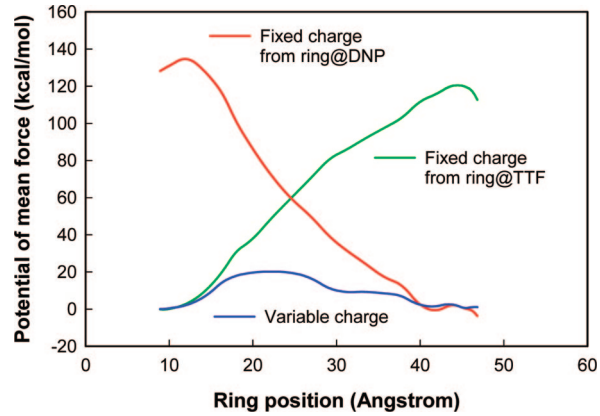

Figure 6. Change of potential of mean force as a function of ring position along the backbone. The blue curve allows the charge to change adiabatically as the ring moves along the dumbbell, which is the reliable result. The other two curves show the error obtained when the charges are fixed: the green curve uses fixed charges from the ring@TTF; the red curve uses a fixed charge from the ring@DNP.

$38.8 \times 0.13/(20)^{1/2} = 1.13$ kcal/mol from integrating over the 38.8 Å distance. Similarly the error of the barrier from the DNP toward the TTF is $25.5 \times 0.13/(14)^{1/2} = 0.89$ kcal/mol from the integration over the 25.5 Å distance. Hence, the small errors in the MF values can lead to substantial errors in the PMF value. However, previous studies that carefully compare various PMF calculation methods show that constraint-biased sampling to determine mean forces is one of the best methods to obtain reasonable PMF values, even though, statistically, they contain large error bars.[52]

3. Results and Discussion

3.1. Charge Scheme: Adiabatic Approximation. We expected that no set of fixed charges scheme would be adequate enough to describe the electrostatic interactions as the highly charged ring is moved along the backbone. Thus, as described in section 2.1, we obtained atomic charges from independent QM at each position as the ring is moved along the backbone. This assumption of adiabatically adjusted charges assumes that charge redistribution is much faster than the time for the ring to travel along the backbone. To test the effect of these charge readjustments on the PMF, Figure 6 shows the PMF based on three different charge schemes for the neutral rotaxane system: the green curve was obtained using the fixed charges from the ring@TTF, the red curve was obtained using the fixed charges from the ring@DNP, and the blue curve was obtained using adiabatic charges.

Clearly, the green and red curves are biased to have a minimum PMF at the position for which the charge was calculated, leading to very bad estimates of the barrier. In contrast, the energy barrier between the TTF and the DNP sites, based on the adiabatic charges, is consistent with experimental observations. Thus, we used the adiabatic charges for all oxidation states from the neutral state to the +2 state.

3.2. Free Energy Profiles from PMF Calculations. Sampling the MFs from the constrained MD simulations (Figure 7a) and integrating them along the ring position, we calculated the profile of the PMF for the shuttling motion of the CBPQT^{4+} ring (Figure 7b). We found that each oxidation state (neutral state (0), oxidized states (+1 and +2)), leads to significantly different profiles.

3.2.1. ΔG_{T2D}**.** We calculated that the most stable complex for the neutral state (black) is CBPQT^{4+}@TTF (ring at 8.9 Å)

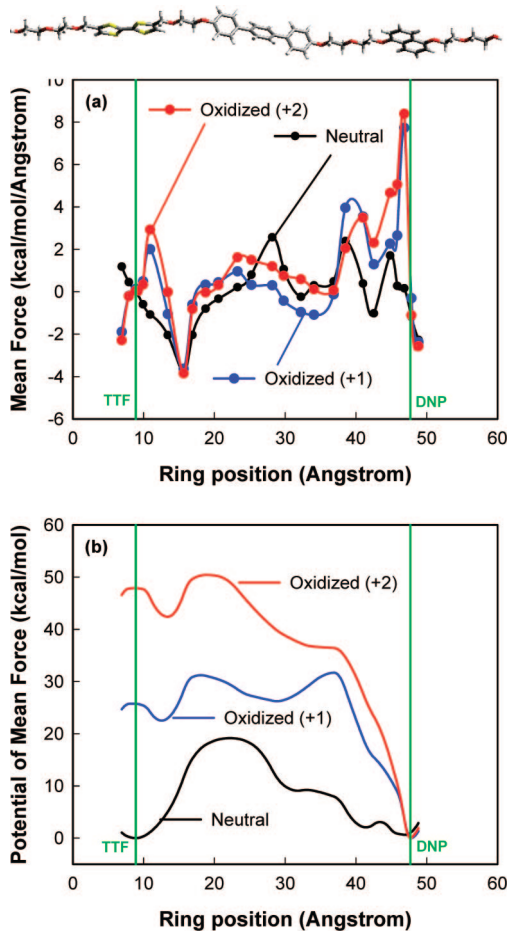

Figure 7. (a) Change of the mean force as a function of ring position along the backbone. (b) Change of the potential of mean force as a function of ring position along the backbone. The green vertical lines denote the ring@TTF (8.90 Å) and ring@DNP (47.70 Å).

whereas the CBPQT^{4+}@DNP state (ring at 47.7 Å) is less stable than the TTF by $\Delta G_{T2D} = 1.0$ kcal/mol. This agrees with various experiments, which lead to $\Delta G_{T2D} = 1.4-1.6$ kcal/mol[15,65−68] on the basis of the difference in the binding free energies of the individual components of the rotaxane in the MeCN solvent. In addition, this calculation agrees with our previous computations from QM ($\Delta G_{T2D} = 2.0$ kcal/mol)[43] and Hessian-based FF calculations ($\Delta G_{T2D} = 2.3$ kcal/mol).[43] We emphasize here that all previous experimental and theoretical studies studied ΔG_{T2D} by comparing the binding free energy of the TTF derivatives with the CBPQT^{4+} ring and the binding free energy of the DNP derivatives with the CBPQT^{4+} ring. Thus, our current calculation is the first direct measurement of the ΔG_{T2D} on a complete rotaxane.

3.2.2. $\Delta G^{\ddagger}_{T2D}$ and $\Delta G^{\ddagger}_{D2T}$ for Neutral Case. We calculate that the free energy barrier is $\Delta G^{\ddagger}_{T2D} = 19.03$ kcal/mol from the TTF toward the DNP, and $\Delta G^{\ddagger}_{D2T} = 18.03$ kcal/mol in the opposite direction. The relaxation barrier in the neutral state was measured for a similar bistable [2]rotaxane in which the triphenylene spacer was missing, leading to[15] (see Table 1)

- $\Delta G^{\ddagger}_{D2T} = 16.2$ kcal/mol ($\tau \sim 0.095$ s) in MeCN solvent
- $\Delta G^{\ddagger}_{D2T} = 18.1$ kcal/mol ($\tau \sim 2.4$ s) in a MeCN/polymethylmethacrylate/propylene carbonate/$LiClO_4$ polymer matrix containing weight ratios of 70:7:20:3
- $\Delta G^{\ddagger}_{D2T} = 22.21$ kcal/mol ($\tau \sim 2.5 \times 10^3$ s) in the molecular-switch tunnel junction

In addition, the devices fabricated with this derivative containing the triphenylene spacer exhibit a relaxation half-life of $\tau \sim 90$ min.[2] ($\Delta G^{\ddagger}_{D2T} = 22.66$ kcal/mol).

In addition, our free energy barrier is quite comparable to the barriers to circumrotation of [2]catenanes. Leigh and coworkers used NMR to determine $\Delta G^{\ddagger}$ of interlocked catenane molecules as 11−20 kcal/mol for various solvents and calculated the free energy barrier as 10−20 kcal/mol using force-field-based Hessians.[69−71]

Although our simulations were performed in the gas phase, the $\Delta G^{\ddagger}_{D2T}$ of 18 kcal/mol agrees well with the experimental barriers (17−22 kcal/mol)[15,34,49] for a variety of environments. This suggests that the energy barrier does not depend strongly on environment.

We did not include the counterions in this study because preliminary calculations showed that the charges would sometimes change in erratic ways due to the floppy energy landscape for the countercharges. Indeed, the good agreement with experiment for the barriers suggests that the instantaneous changes in the potential due to counterions can be neglected.

3.2.3. $\Delta G^{\ddagger}_{T2D}$ and $\Delta G^{\ddagger}_{D2T}$ for Oxidized Cases. Although the neutral state prefers to have the CBPQT^{4+} ring at the TTF, we find that the +1 and +2 oxidized states lead to a completely different energy profile (Figure 7b). In both cases, the DNP becomes the global minimum with the TTF destabilized by $\Delta G = 25.75$ kcal/mol for the +1 oxidation state and $\Delta G = 47.78$ kcal/mol for the +2 oxidation state.

Starting with the ring at the TTF site and oxidizing, we find that the ring moves first by ~5 Å to a local minimum on the ethylene oxide linker (with an energy decrease by $\Delta G = 3.25$ kcal for the +1 and $\Delta G = 5.49$ kcal/mol for the +2). Then, it has a free energy barrier of $\Delta G = 8.70$ kcal/mol (+1 state) or 8.02 kcal/mol (+2 state) to continue past the triphenylene spacer and toward the DNP for oxidation states.

Using the Eyring rate equation [$1/\tau = (k_B T/h) \exp(-\Delta G^{\ddagger}/RT)$], the time required to overcome this barrier to move onto the DNP is 2.9×10^{-7} s for the +1 oxidation state and 9.0×10^{-8} s for the +2 oxidation state. It would be interesting to design an experiment to probe for this predicted barrier. It has been assumed that the huge Coulomb potential of the +4 ring with the +2 TTF would preclude a barrier. The origin of this barrier in the oxidized state is discussed below, which we find arises from the triphenylene spacer. We expect that there would be no barrier without this spacer.

Relative to the final state of the ring at the DNP site, the energy at the ethylene oxide linker (EO) near the TTF site is 22.52 kcal/mol higher (+1 oxidation), leading to a Boltzmann population of 10^{-17}. For the +2 oxidation state, the energy is 42.41 kcal/mol higher, leading to a population of 10^{-32}. Thus, for oxidation states +1 and +2, we expect the CBPQT^{4+} ring to stay on the DNP site until the system is reduced.

Indeed, there is an experimental estimate of this reverse barrier. Using a modified AFM with the ring attached, Brough et al.[72] measured the force exerted on the ring shuttling from the DNP to the TTF in the +2 oxidized system as 145 pN. Combining this experimental data with results from molecular mechanics simulations, they estimated the energy barrier to be 65 kcal/mol. This can be compared to our calculated barrier of 50.4 kcal/mol energy, validating the accuracy of the experiment. The maximum force measured in our simulation during the ring shuttling is 583 pN, which is similar to the experimental value of 145 pN.

3.3. Effect of Coulombic Energy and van der Waals Energy. To understand why the PMF profiles are so different between the neutral, +1, and +2 oxidation states, we calculated

TABLE 1: Free Energy Barriers, Rate Constants, and Relaxation Half-Lives from DNP toward TTF (DNP → TTF) at 298 K (All Simulation Results from this Work)

			condition	
ΔG (kcal/mol)	k (s^{-1})[a]	$\tau_{1/2}$ (s)[a]		
18.03 ± 1.5 (simulation)	0.33 ± 0.83	2.1 ± 5.4	neutral	gas phase solution
16.2 ± 0.3 (exp[34])	7.3 ± 3.7	0.095 ± 0.048	neutral	(CH_3CN)
18.1 ± 0.2 (exp[15,34,71])	0.3 ± 0.10	2.4 ± 0.082	neutral	polymer matrix[b]
22.21 ± 0.04 (exp[15,34,71])	(2.7 ± 0.19) × 10^{-4}	(2.5 ± 0.18) × 10^{3}	neutral	molecular-switch junction
31.22 (simulation)	6.3 × 10^{-11}	1.1 × 10^{10}	oxidation +1	gas phase
50.43 (simulation)	4.5 × 10^{-25}	1.5 × 10^{24}	oxidation +2	gas phase
65 kcal/mol (exp + simulation[72])			oxidation +2	SAM on SiO_2 wafers[c]

[a] Values are calculated using the Eyring equation, $1/\tau = (k_B T/h) \exp(-\Delta G^{\ddagger}/RT)$. [b] Weight ratio 70:7:20:3 for CH_3CN/poly(methyl methacrylate)/propylene carbonate/$LiClO_4$. [c] The modified AFM tip is attached to the CBPQT4+ ring.

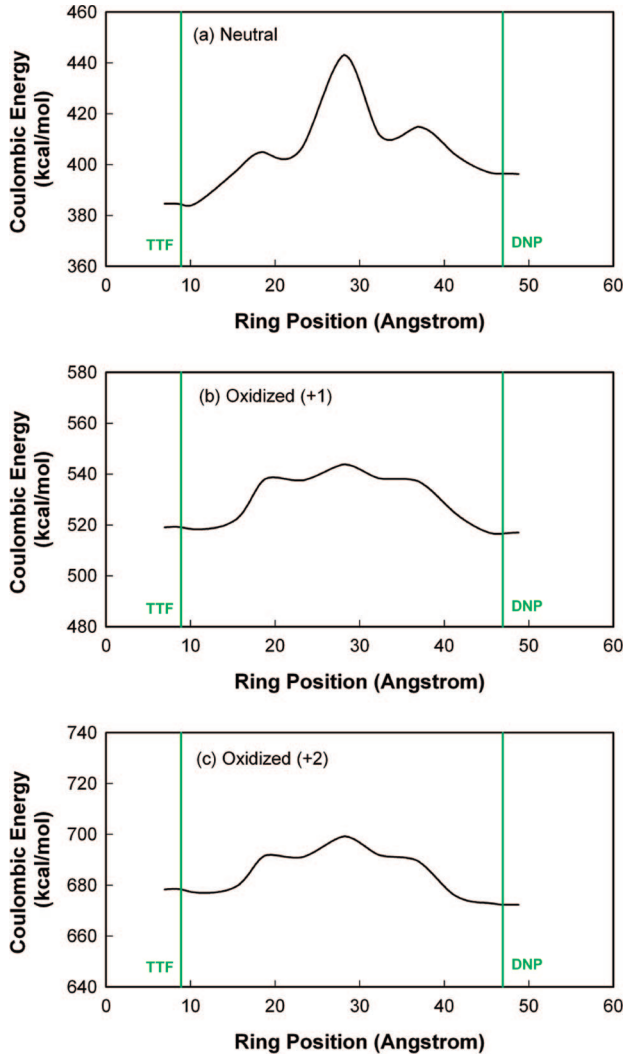

Figure 8. Change of Coulombic interaction energy as a function of the ring position: (a) neutral state; (b) oxidation state +1; (c) oxidation state +2.

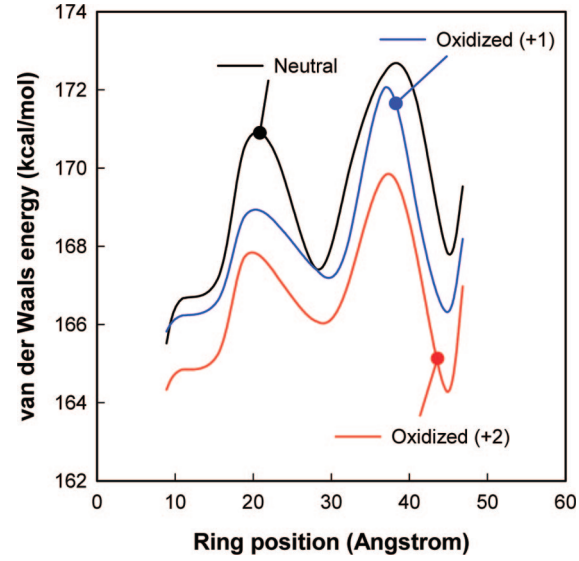

Figure 9. Change of van der Waals interaction energy as a function of the ring position: (a) neutral state; (b) oxidation state +1; (c) oxidation state +2.

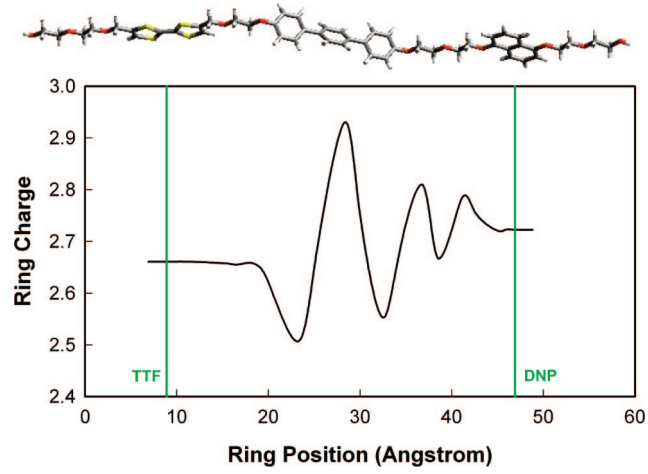

Figure 10. Variations in the total charge on the ring as a function of the ring position for the neutral case.

the change in the Coulombic interaction energy and the van der Waals (vdW) interaction energy as a function of ring position along the backbone, for these three oxidation states (Figures 8 and 9).

For the neutral state, we find that the Coulombic energy increases by 60 kcal/mol as the ring moves from the TTF to the triphenylene spacer (barrier) and then drops by 45 kcal/mol as it moves to the DNP. On the other hand, the vdW energy changes, within a range of ±4 kcal/mol, while the ring travels from the TTF to the DNP.

This indicates that the barrier is dominated by the differential Coulombic interactions with a peak of 443 kcal/mol at $z = 28$Å (over the spacer). We were quite surprised because we expected the barrier to be dominated by vdW repulsions due to the bulky size of the triphenylene. To understand why Coulombic interactions are so important, we plot in Figure 10 the total charge on the ring along the pathway, in the neutral case. We see that at the TTF or the DNP positions there is strong delocalization from the ring onto the backbone, but as the ring passes over the

triphenylene spacer (at $z = 28$ Å), this charge localizes back onto the ring. Thus, we conclude that localization of the ring charge increases the Coulombic repulsion and dominates the free energy barrier. This suggests that the barrier can be modified dramatically by changing the polarity of the spacer.

We also found that as the system is oxidized, the magnitude of Coulombic repulsion increases from 380−445 kcal/mol for the neutral state, to 520−545 kcal/mol for the +1 oxidation state, and finally, to 670−700 kcal/mol for the +2 oxidation state. In contrast, the vdW energy changes from 165−173 to 165−172 to 164−171 kcal/mol as the system is oxidized. This implies that the driving force inducing the mechanical movement of the ring is the increased Coulombic repulsion due to oxidization of the rotaxane. This confirms our view since the beginning of our experiments.

However, the PMF profile (Figure 6b) still differs substantially from the Coulombic energy profile (Figure 8). For instance, in the neutral case, the Coulombic energy difference between two stations is 12.03 kcal/mol, which is ∼12 times larger than $\Delta G_{T2D} = 1.0$ kcal/mol, and the Coulombic energy barrier for the shuttling from the DNP to the TTF is 46.75 kcal/mol, which is ∼2.6 times larger than $\Delta G^{\ddagger}_{D2T} = 18.03$ kcal/mol. Thus, the key features of the PMF profile are not fully explained in terms of the Coulombic energy alone. Another possible contributor to the free energy is vibrational entropy, which can be investigated directly from the MD simulation trajectory.[73,74]

4. Summary

We used constrained MD simulations to calculate the free energy profile at 300 K for the shuttling of the $CBPQT^{4+}$ ring between the TTF and the DNP in the rotaxane molecule. This free energy profile was derived by calculating and integrating the MF acting on the ring as it is moved from one position to another position along the backbone. We found that it is particularly important to allow the charges to adjust adiabatically as the ring moves. Indeed, we find that the Coulomb interactions dominate the barriers for these systems.

We found that the free energy barrier from the DNP to the TTF is 18.03 kcal/mol for the neutral system, which agrees well with experimental values of 17−22 kcal/mol for various environments. We calculate that the ΔG between the TTF and the DNP positions is 1.0 kcal/mol, which compares well with experimental results of 1.4−1.6 kcal/mol obtained from binding energies of separate DNP and TTF systems with the $CBPQT^{4+}$ ring.

These results validate the accuracy of our computational procedure. Thus, we can now use this validated technique for estimating the switching kinetics for new designs of molecular architectures.

Acknowledgment. The computational work was initiated with support by the National Science Foundation (NIRT, W.A.G.). The collaboration was supported by the Microelectronics Advanced Research Corporation (MARCO; W.A.G. and J.F.S.) and its Focus Centers on Functional Engineered NanoArchitectonics (FENA) and Materials Structures and Devices, the Molectronics Program of the Defense Advanced Research Projects Agency (DARPA; J.F.S. and J.R.H.), the Center for Nanoscale Innovation for Defense (CNID; J.F.S.), and the MARCO Materials Structures and Devices Focus Center (J.R.H.). In addition, the facilities of the MSC (W.A.G.) were supported by ONR-DURIP and ARO-DURIP.

Supporting Information Available: Figures of probability density functions and chemical structures. Table of partial charge distributions. This material is available free of charge via the Internet at http://pubs.acs.org.

References and Notes

(1) Luo, Y.; Collier, C. P.; Jeppesen, J. O.; Nielsen, K. A.; Delonno, E.; Ho, G.; Perkins, J.; Tseng, H. R.; Yamamoto, T.; Stoddart, J. F.; Heath, J. R. *ChemPhysChem* **2002**, *3*, 519–525.

(2) Green, J. E.; Choi, J. W.; Boukai, A.; Bunimovich, Y.; Johnston-Halperin, E.; DeIonno, E.; Luo, Y.; Sheriff, B. A.; Xu, K.; Shin, Y. S.; Tseng, H.-R.; Stoddart, J. F.; Heath, J. R. *Nature* **2007**, *445*, 414–417.

(3) Anelli, P. L.; Spencer, N.; Stoddart, J. F. *J. Am. Chem. Soc.* **1991**, *113*, 5131–5133.

(4) Bissell, R. A.; Cordova, E.; Kaifer, A. E.; Stoddart, J. F. *Nature* **1994**, *369*, 133–137.

(5) Asakawa, M.; Ashton, P. R.; Balzani, V.; Credi, A.; Hamers, C.; Mattersteig, G.; Montalti, M.; Shipway, A. N.; Spencer, N.; Stoddart, J. F.; Tolley, M. S.; Venturi, M.; White, A. J. P.; Williams, D. J. *Angew. Chem. Int. Ed.* **1998**, *37*, 333–337.

(6) Balzani, V.; Credi, A.; Mattersteig, G.; Matthews, O. A.; Raymo, F. M.; Stoddart, J. F.; Venturi, M.; White, A. J. P.; Williams, D. J. *J. Org. Chem.* **2000**, *65*, 1924–1936.

(7) Collier, C. P.; Mattersteig, G.; Wong, E. W.; Luo, Y.; Beverly, K.; Sampaio, J.; Raymo, F. M.; Stoddart, J. F.; Heath, J. R. *Science* **2000**, *289*, 1172–1175.

(8) Barboiu, M.; Lehn, J.-M. *Proc. Natl. Acad. Sci. U.S.A.* **2002**, *99*, 5201–5206.

(9) Hogg, L.; Leigh, D. A.; Lusby, P. J.; Morelli, A.; Parsons, S.; Wong, J. K. Y. *Angew. Chem., Int. Ed.* **2004**, *43*, 1218–1221.

(10) Zheng, X.; Mulcahy, M. E.; Horinek, D.; Galeotti, F.; Magnera, T. F.; Michl, J. *J. Am. Chem. Soc.* **2004**, *126*, 4540–4542.

(11) Hawthorne, M. F.; Zink, J. I.; Skelton, J. M.; Bayer, M. J.; Liu, C.; Livshits, E.; Baer, R.; Neuhauser, D. *Science* **2004**, *303*, 1849–1851.

(12) de Jong, J. J. D.; Lucas, L. N.; Kellogg, R. M.; van Esch, J. H.; Reringa, B. L. *Science* **2004**, *304*, 278–281.

(13) Turberfield, A. J.; Mitchell, J. C.; Yurke, B.; Mills, A. P.; Blakey, M. I.; Simmel, F. C. *Phys. Rev. Lett.* **2003**, *90*, art. no.118102.

(14) Liu, H. Q.; Schmidt, J. J.; Bachand, G. D.; Rizk, S. S.; Looger, L. L.; Hellinga, H. W.; Montemagno, C. D. *Nat. Mater.* **2002**, *1*, 173–177.

(15) Choi, J. W.; Flood, A.; Steuerman, D. W.; Nygaard, S.; Braunschweig, A.; Moonen, N.; Laursen, B.; Luo, Y.; DeIonno, E.; Peters, A. J.; Jeppesen, J. O.; Stoddart, J. F.; Heath, J. R. *Chem. Eur. J.* **2006**, *12*, 261–279.

(16) Collier, C. P.; Jeppesen, J. O.; Luo, Y.; Perkins, J.; Wong, E. W.; Heath, J. R.; Stoddart, J. F. *J. Am. Chem. Soc.* **2001**, *123*, 12632–12641.

(17) Diehl, M. R.; Steuerman, D. W.; Tseng, H. R.; Vignon, S. A.; Star, A.; Celestre, P. C.; Stoddart, J. F.; Heath, J. R. *ChemPhysChem* **2003**, *4*, 1335–1339.

(18) Credi, A.; Balzani, V.; Langford, S. J.; Stoddart, J. F. *J. Am. Chem. Soc.* **1997**, *119*, 2679–2681.

(19) Collier, C. P.; Wong, E. W.; Belohradsky, M.; Raymo, F. M.; Stoddart, J. F.; Kuekes, P. J.; Williams, R. S.; Heath, J. R. *Science* **1999**, *285*, 391–394.

(20) Elizarov, A. M.; Chiu, S. H.; Stoddart, J. F. *J. Org. Chem.* **2002**, *67*, 9175–9181.

(21) Carroll, R. L.; Gorman, C. B. *Angew. Chem. Int. Ed.* **2002**, *41*, 4379–4400.

(22) Yu, H. B.; Luo, Y.; Beverly, K.; Stoddart, J. F.; Tseng, H. R.; Heath, J. R. *Angew. Chem. Int. Ed.* **2003**, *42*, 5706–5711.

(23) Heath, J. R.; Ratner, M. A. *Phys. Today* **2003**, *56*, 43–49.

(24) Balzani, V.; Gomez-Lopez, M.; Stoddart, J. F. *Acc. Chem. Res.* **1998**, *31*, 405–414.

(25) Balzani, V.; Credi, A.; Raymo, F. M.; Stoddart, J. F. *Angew. Chem. Int. Ed.* **2000**, *39*, 3349–3391.

(26) Chia, S. Y.; Cao, J. G.; Stoddart, J. F.; Zink, J. I. *Angew. Chem. Int. Ed.* **2001**, *40*, 2447–2451.

(27) Belohradsky, M.; Elizarov, A. M.; Stoddart, J. F. *Collect. Czech. Chem. Commun.* **2002**, *67*, 1719–1728.

(28) Hernandez, R.; Tseng, H. R.; Wong, J. W.; Stoddart, J. F.; Zink, J. I. *J. Am. Chem. Soc.* **2004**, *126*, 3370–3371.

(29) Badjic, J. D.; Balzani, V.; Credi, A.; Silvi, S.; Stoddart, J. F. *Science* **2004**, *303*, 1845–1849.

(30) Tseng, H. R.; Vignon, S. A.; Stoddart, J. F. *Angew. Chem., Int. Ed.* **2003**, *42*, 1491–1495.

(31) Jeppesen, J. O.; Perkins, J.; Becher, J.; Stoddart, J. F. *Angew. Chem. Int. Ed.* **2001**, *40*, 1216–1221.

(32) Jeppesen, J. O.; Nielsen, K. A.; Perkins, J.; Vignon, S. A.; Di Fabio, A.; Ballardini, R.; Gandolfi, M. T.; Venturi, M.; Balzani, V.; Becher, J.; Stoddart, J. F. *Chem. Eur. J.* **2003**, *9*, 2982–3007.

(33) Yamamoto, T.; Tseng, H. R.; Stoddart, J. F.; Balzani, V.; Credi, A.; Marchioni, F.; Venturi, M. *Collect. Czech. Chem. Commun.* **2003**, *68*, 1488–1514.

(34) Tseng, H. R.; Vignon, S. A.; Celestre, P. C.; Perkins, J.; Jeppesen, J. O.; Di Fabio, A.; Ballardini, R.; Gandolfi, M. T.; Venturi, M.; Balzani, V.; Stoddart, J. F. *Chem. Eur. J.* **2004**, *10*, 155–172.

(35) Kang, S. S.; Vignon, S. A.; Tseng, H. R.; Stoddart, J. F. *Chem. Eur. J.* **2004**, *10*, 2555–2564.

(36) Livoreil, A.; Dietrichbuchecker, C. O.; Sauvage, J. P. *J. Am. Chem. Soc.* **1994**, *116*, 9399–9400.

(37) Flood, A. H.; Peters, A. J.; Vignon, S. A.; Steuerman, D. W.; Tseng, H.-R.; Kang, S.; Heath, J. R.; Stoddart, J. F. *Chem. Eur. J.* **2004**, *24*, 6558–6561.

(38) Steuerman, D. W.; Tseng, H.-R.; Peters, A. J.; Flood, A. H.; Jeppesen, J. O.; Nielsen, K. A.; Stoddart, J. F.; Heath, J. R. *Angew. Chem. Int. Ed.* **2004**, *43*, 6486–6491.

(39) Lee, I. C.; Frank, C. W.; Yamamoto, T.; Tseng, H.-R.; Flood, A. H.; Stoddart, J. F.; Jeppesen, J. O. *Langmuir* **2004**, *20*, 5809–5828.

(40) Tseng, H. R.; Wu, D. M.; Fang, N. X. L.; Zhang, X.; Stoddart, J. F. *ChemPhysChem* **2004**, *5*, 111–116.

(41) Raehm, L.; Kern, J. M.; Sauvage, J. P.; Hamann, C.; Palacin, S.; Bourgoin, J. P. *Chem. Eur. J.* **2002**, *8*, 2153–2162.

(42) Jang, Y. H.; Kim, Y. H.; Jang, S. S.; Hwang, S. G.; Goddard, W. A., III *Abstr. Pap., Am. Chem. Soc.* **2004**, *227*, U850−U850.

(43) Jang, S. S.; Jang, Y. H.; Kim, Y.-H.; Goddard, W. A., III; Flood, A. H.; Laursen, B. W.; Tseng, H.-R.; Stoddart, J. F.; Jeppesen, J. O.; Choi, J. W.; Steuerman, D. W.; DeIonno, E.; Heath, J. R. *J. Am. Chem. Soc.* **2005**, *127*, 1563–1575.

(44) Jang, S. S.; Jang, Y. H.; Kim, Y. H.; Goddard, W. A., III; Choi, J. W.; Heath, J. R.; Laursen, B. W.; Flood, A. H.; Stoddart, J. F.; Norgaard, K.; Bjornholm, T. *J. Am. Chem. Soc.* **2005**, *127*, 14804–14816.

(45) Jang, Y. H.; Jang, S. S.; Goddard, W. A., III *J. Am. Chem. Soc.* **2005**, *127*, 4959–4964.

(46) Jang, Y. H.; Goddard, W. A., III *J. Phys. Chem. B* **2006**, *110*, 7660–7665.

(47) Kim, Y.-H.; Goddard, W. A., III *J. Phys. Chem. C* **2007**, *111*, 4831–4837.

(48) Jeppesen, J. O.; Nygaard, S.; Vignon, S. A.; Stoddart, J. F. *Eur. J. Org. Chem.* **2004**, *196*, 220.

(49) Dichtel, W. R.; Heath, J. R.; Stoddart, J. F. *Philos. Trans. R. Soc. A, Math. Phys. Eng. Sci.* **2007**, *365*, 1607–1625.

(50) Carter, E. A.; Ciccotti, G.; Hynes, J. T.; Kapral, R. *Chem. Phys. Lett.* **1989**, *156*, 472–477.

(51) Sprik, M.; Ciccotti, G. *J. Chem. Phys.* **1998**, *109*, 7737–7744.

(52) Trzesniak, D.; Kunz, A. P. E.; van Gunsteren, W. F. *ChemPhysChem* **2007**, *8*, 162–169.

(53) *Jaguar*, V. 5.0 ed.; Schroedinger Inc.: Portland, 2003.

(54) Evans, D. J.; Morriss, G. P. *Statistical Mechanics of Nonequilibrium Liquids*; Academic Press: London, 1990.

(55) Fixman, M. *Proc. Natl. Acad. Sci. U.S.A.* **1974**, *71*, 3050–3053.

(56) Mayo, S. L.; Olafson, B. D.; Goddard, W. A., III *J. Phys. Chem.* **1990**, *94*, 8897–8909.

(57) Jang, S. S.; Molinero, V.; Cagin, T.; Goddard, W. A., III *J. Phys. Chem. B* **2004**, *108*, 3149–3157.

(58) Jang, S. S.; Lin, S.-T.; Cagin, T.; Molinero, V.; Goddard, W. A., III *J. Phys. Chem. B* **2005**, *109*, 10154–10167.

(59) Jang, S. S.; Goddard, W. A. *J. Phys. Chem. C* **2007**, *111*, 2759–2769.

(60) Jang, S. S.; Lin, S.-T.; Maiti, P. K.; Blanco, M.; Goddard, W. A., III; Shuler, P.; Tang, Y. *J. Phys. Chem. B* **2004**, *108*, 12130–12140.

(61) Jang, S. S.; Goddard, W. A. *J. Phys. Chem. B* **2006**, *110*, 7992–8001.

(62) Plimpton, S. J. *J. Comput. Phys.* **1995**, *117*, 1–19.

(63) Plimpton, S. J.; Pollock, R.; Stevens, M. *The Eighth SIAM Conference on Parallel Processing for Scientific Computing Minneapolis*; 1997.

(64) Swope, W. C.; Andersen, H. C.; Berens, P. H.; Wilson, K. R. *J. Chem. Phys.* **1982**, *76*, 637–649.

(65) Castro, R.; Nixon, K. R.; Evanseck, J. D.; Kaifer, A. E. *J. Org. Chem.* **1996**, *61*, 7298–7303.

(66) Ashton, P. R.; Balzani, V.; Becher, J.; Credi, A.; Fyfe, M. C. T.; Mattersteig, G.; Menzer, S.; Nielsen, M. B.; Raymo, F. M.; Stoddart, J. F.; Venturi, M.; Williams, D. J. *J. Am. Chem. Soc.* **1999**, *121*, 3951–3957.

(67) Bryce, M. R.; Cooke, G.; Duclairoir, F. M. A.; Rotello, V. M. *Tetrahedron Lett.* **2001**, *42*, 1143–1145.

(68) Nielsen, M. B.; Jeppesen, J. O.; Lau, J.; Lomholt, C.; Damgaard, D.; Jacobsen, J. P.; Becher, J.; Stoddart, J. F. *J. Org. Chem.* **2001**, *66*, 3559–3563.

(69) Leigh, D. A.; Murphy, A.; Smart, J. P.; Deleuze, M. S.; Zerbetto, F. *J. Am. Chem. Soc.* **1998**, *120*, 6458–6467.

(70) Leigh, D. A.; Troisi, A.; Zerbetto, F. *Chem. Eur. J.* **2001**, *7*, 1450–1454.

(71) Deleuze, M. S.; Leigh, D. A.; Zerbetto, F. *J. Am. Chem. Soc.* **1999**, *121*, 2364–2379.

(72) Brough, B.; Northrop, B. H.; Schmidt, J. J.; Tseng, H. R.; Houk, K. N.; Stoddart, J. F.; Ho, C. M. *Proc. Natl. Acad. Sci. U.S.A.* **2006**, *103*, 8583–8588.

(73) Lin, S. T.; Blanco, M.; Goddard, W. A. *J. Chem. Phys.* **2003**, *119*, 11792–11805.

(74) Lin, S. T.; Jang, S. S.; Cagin, T.; Goddard, W. A. *J. Phys. Chem. B* **2004**, *108*, 10041–10052.

JP809213M